

This is a postprint version of the following published document:

Alcántara-García, A.; García-Casas, A.; Jiménez-Morales, A.
(2020) The effect of the organosilane content on the barrier
features of sol-gel anticorrosive coatings applied on carbon
steel, *Progress in Organic Coatings*, v. 139, 105418.

DOI: <https://doi.org/10.1016/j.porgcoat.2019.105418>

© 2019 Elsevier B.V. All rights reserved.



This work is licensed under a [Creative Commons AttributionNonCommercialNoDerivatives 4.0 International License](https://creativecommons.org/licenses/by-nc-nd/4.0/)

The effect of the organosilane content on the barrier features of sol-gel anticorrosive coatings applied on carbon steel

A. Alcantara-García^{a,*}, A. García-Casas^a, A. Jiménez-Morales^{a,b}

^a *Departamento de Ciencia e Ingeniería de Materiales e Ingeniería Química, Universidad Carlos III de Madrid, Av. Universidad, 30, 28911 Leganés, Madrid, Spain*

^b *Instituto Tecnológico de Química y Materiales Álvaro Alonso Barba, de la Universidad Carlos III de Madrid, Spain*

ABSTRACT

The main objective of this work was to determine the influence of the molar ratio of two compounds on the structure of the molecular net synthesized by sol-gel technology for the protection corrosion coating on carbon steel. Three different molar ratios were used to prepare the organic-inorganic hybrid materials by hydrolysis and condensation of (3-glycidyloxypropyl)trimethoxysilane (GPTMS) and tetraethylorthosilane (TEOS) in an ethanol/water solution. The behavior of the three different syntheses was evaluated by chemical, physical, and electrochemical methods. The evolution of the synthesis was determined by FT-IR and viscosity until the optimal moment prior to apply the sol to the metallic substrate. Chemical cross-linking of xerogel was determined by solid state of ²⁹Si-NMR and the behavior on thermal stability is given by TGA analysis. Samples of carbon steel were coated by the synthesis and the coatings were characterized using scanning electrochemical microscopy (SEM) finding considerable differences between the three coatings. Potentiodynamic polarization and impedance measurements were carried out to study the effect of the corrosion resistance of the synthesis in 10mM NaCl solution.

Introduction

Sol-gel technology has been developing in the past 50 years due to a growing demand in industrial, engineering, and medical fields. This technology consists on an extremely versatile synthesis for the production of ceramic and glass materials. Synthesis of nanoparticles, inorganic encapsulation of active materials and development of multifunctional surfaces using deposition of coatings, are examples of the multiple application of this technique. Through both well-known chemical reactions hydrolysis and condensation (Fig. 1) the sol-gel process experiments the transition of a system from a liquid phase (sol) to a solid phase (gel). Alkoxysilanes are the most widely used metal-organic precursors for the preparation of materials by sol-gel processing. During the first reaction, hydrolysis, the silane alkoxide bond (Si-OR) results in the formation of a silanol (Si-OH). Once this reaction has taken place, two silanols can combine deleting a water molecule in the condensation reaction and form an inorganic highly dense silica network by means of siloxane bonds (Si-O-Si) [1-5].

At the beginning, the sol-gel route was focused on the synthesis of pure inorganic materials being TEOS the classical inorganic precursor. However, through time, several researchers have probed the benefits of organic-inorganic hybrid materials which are obtained from the structural incorporation of organic groups, such as epoxy, amine, vinyl, acrylic, etc., via Si-C bonds within the sol-gel precursors. These hybrids offer the possibility to combine both properties; on one hand inorganic (hardness, chemical resistance, adhesion to the substrate...) and on the other hand the organic ones (elasticity, toughness, low curing temperatures...) [3,5]. Several factors influence the final chemical structure of the silanes and

therefore their properties, such as pH, curing time, aging concentration and chemical structure of the silanes. Therefore, depending on the selected precursors and its molar ratio, it is possible to obtain hybrid layers with variable mechanical properties [6–9].

One of the most important research fields for these hybrid organic-inorganic materials has been in the application of sol-gel coatings onto metal surfaces to serve as a protective barrier against corrosive species. Various techniques to apply a sol-gel coating can be used being the most commonly ones dip-coating and spin-coating, but also spraying and electrodeposition [10]. After the deposition of the coating the materials are subjected to a curing step that can produce the appearance of cracks on the surface due to the contraction of volume and internal stress accumulating during solvent and water evaporation [5,10]. Electrolyte and aggressive species can diffuse through cracks and small defects like pores or scratches on the coatings archiving the metal Surface and starting corrosion processes. Therefore, corrosion resistance of the sol-gel coating is directly related with the physical barrier properties and with its chemical structure [11].

In this work, the influence of different proportions of organic/inorganic silanes was studied. Chemical structure and physical properties were evaluated in order to improve the corrosion resistance, which has been measured by polarization test and electrochemical impedance spectroscopy (EIS).

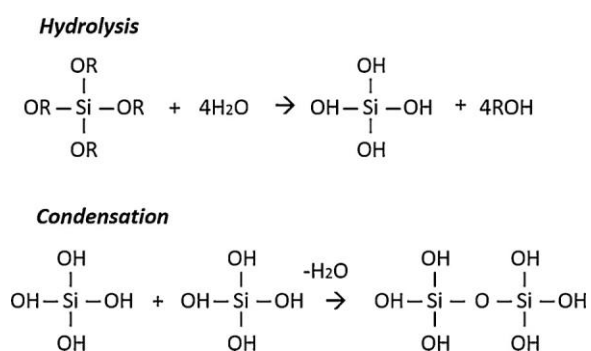


Fig. 1. Hydrolysis and condensation scheme

Experimental

Materials and sample preparation

Carbon steel substrates (C 0.045 wt.% ; Mn 0.33 wt.% ; Si 0.01 wt.%; P 0.018 wt.%; S 0.09 wt.%) were provided by Espan color, S.L. and cut in samples of 50×20×2 mm³. Metallic substrates, without polishing, were ultrasonically cleaned in alcohol for 15 min and dried at room temperature. Three sols were prepared by varying the molar ratio of the organopolysiloxanes: 1 mol of tetraethylorthosilane (TEOS, 98% from Sigma-Aldrich) and 1 mol of (3-glycidyloxypropyl)trimethoxysilane (GPTMS, 98% from Sigma-Aldrich) for synthesis TG11; 1 mol of TEOS and 2 mol of GPTMS for synthesis TG12; and 2 mol of TEOS and 1 mol of GPTMS for synthesis TG21. Ethanol and water were added in a molar ratio silane/ethanol/water of 1/3/3. All the organic species were mixed before the addition of acidified water (with HNO₃ pH=1). Table 1 summarizes the prepared syntheses. Sols were stirred at room temperature for 3 days. The protective layer was applied on the Steel samples by dipping them into the solutions for 15 s at 100 mm · min⁻¹ and retracting them with the same speed. Finally, samples were dried at room temperature for 60 min, followed by thermal treatment at 60 °C for 17 h inside an oven.

Instruments

The evolution of the hydrolysis-condensation reaction was monitored by FTIR spectral analysis. Each sample was prepared by adding a sol-gel synthesis's drop to a pressed KBr disc. Spectra were recorded with a Perkin Elmer spectrum GX FT-IR System at room temperature covering the wave number range of 4000–500 cm^{-1} and with a resolution of 8 cm^{-1} . The viscosity of sols was measured using a HAAKE ViscotesterIQ from Thermo Scientific with parallel plate geometry and profiled surfaces. Viscosity was recorded for 30 s at fixed shear rates of 100, 200, 300, 400, 500, 600, 700, 800 and 900 s^{-1} . Similar and stable values were obtained with the different applied share rates and a mean viscosity value from all the tests was calculated. The viscosity of each sol was evaluated at different times of reaction, namely 1, 4, 8, 24, 48 and 72 h. Gels were dried in the oven at 60 °C for 17 h and ground in an agate mortar prior to their characterization by TGA and ^{29}Si -NMR. TGA measures were performed using the model Pyris™ 1 TGA from PerkinElmer. Around 20 mg of the dry gel (xerogel) was placed on alumina crucibles and heated at a 10 °C/min rate from 30 °C to 850 °C in air atmosphere. Measurements were made by duplicated. The ^{29}Si -NMR spectra were recorded in a Bruker AVANCE 400 spectrometer equipped with fast Fourier transform unit. Frequency used was 79.48 MHz (9.4 T). Samples were spun at 10 kHz around an axis inclined 54o44' with respect to the external magnetic field. Spectra were acquired with a pulse length of 5 μs (90° pulse), a relaxation delay of 10 s was used and 6000 accumulations were acquired. Spectra were referenced to TMS. The water contact angle of coatings was determined by measuring the static contact angle of deionized water onto sol–gel surfaces using an automatic contact angle meter OCA 15 plus DATAPHYSICS. A sessile drop of 4 μl was deposited on the surfaces at room temperature. The water contact angle was determined by the half angle method and at least on 2 different locations per sample. The given value is the mean of at least 5 measurements. To examine the surface and cross-sectional morphologies of the coated samples, scanning electron microscope SEM, Teneo FEI microscope with W filament was used. Images were captured applying 5 Kv and 0.2 nA. Small sections of the samples (1×1 cm^2) were cut out using a diamond saw, then the samples were embedded in a polyester resin, polished and cover by Copper. Electrochemical measurements were performed using AUTOLAB PGSTAT302 N. All experiments were conducted at room temperature (20.5 °C \pm 0.5 °C) in the conventional three-electrode cell arrangement, using an Ag/AgCl/KCl (3 M) electrode as reference ($E_0 = +0.210$ V vs. NHE), a platinum wire as counter electrode and a surface area of 0.38 cm^2 of the working electrode (the testing specimens) was exposed to an electrolyte of 10mM NaCl. The cell was placed in a Faraday cage to avoid external interferences from electromagnetic fields and wandering currents. Potentiodynamic polarization curves were recorded from -500 mV to 500 mV with respect to the Open Circuit Potential (OCP) using a scan rate of 0.116 mV/s after 60 min of stabilization. In impedance tests, the samples were left unpolarised for 24 h to attain a stable OCP in the testing solution (10mM NaCl). Signals were subsequently recorded at regular intervals for 24 h using an amplitude of 10 mV with respect to OCP, and a frequency scan ranging from 100 kHz to 10 mHz. Impedances are spaced logarithmically with 5 points per decade. OCP was recorded for 10 min before and after each impedance measurement in order to monitor the stability of the coatings EIS data were fitted and analyzed in terms of equivalent circuits (EC) using ZView software (Scribner Associates, Charlottesville, VA, USA) to obtain the most relevant impedance parameters.

Table 1

Summary of the prepared sol-gel syntheses.

Nomenclature	TEOS:GPTMS/molar ratio
Uncoated Steel	–
TG11	1:1
TG12	1:2
TG21	2:1

Results and discussion

Characterization of hybrid sols

Fig. 2 depicts the FTIR spectra of the three syntheses prepared at 24 h of reaction time. The spectrum of one synthesis, TG11, before the addition of water is shown to better appreciate the evolution of bands during hydrolysis and condensation. In Fig. 2 this spectrum is labelled as un-reacted synthesis. All syntheses showed the same spectrum prior to the addition of water. The formation of SiOH bonds created due to hydrolysis reaction are revealed at 3340 cm^{-1} (peak A) and 950 cm^{-1} (peak D) [12–14]. Whereas, the formation of SiOeSi bonds related to the condensation reaction is reflected by the bands observed between 1000–1200 cm^{-1} (peak C and B) [3,13,15,16]. The correlation between each signal and the formation of the different bonds is summarized in Table 2. FTIR experiments reveal that different proportion of organosilane does not affect the evolution of the hydrolysis and condensation reactions. The spectra of the three syntheses have the same characteristics bands corresponding to hydrolysis and condensation reactions at 24 h meaning that these reactions are not affected by the initial molar ratio of precursors. The evolution of viscosity with time for each sol is depicted in Fig. 3. The viscosity of the three syntheses gradually increased from the beginning to 48 h and shifted to values on the order of magnitude of 100 $\text{mPa} \cdot \text{s}$ at 72 h. Therefore, the condensation kinetics of the reaction was found to be independent of the molar ratio of the precursors. In order to obtain the highest thickness, which will lead to better barrier features if the coating surface is free of cracks, the substrates were covered by dipping them into the sols at their highest viscosity, 72 h for all the studied sols. Viscosity optimization is an important step because this factor is directly related to the thickness of the coating. Higher viscosity implies higher thickness of the physical barrier to protect the metal surface against corrosion atmosphere, however this could also provoke a lack of hydroxyl groups necessary to attach the metallic surface giving low adherence. Thus, the viscosity of sols is a relevant parameter that allows tailoring the thickness of coatings avoiding the loss of adhesion to the metallic substrate [17].

Characterization of xerogels

Thermogravimetric analysis for the three xerogels and their first derivate are pictured in Fig. 4. Three steps were identified in the complete degradation process of the three xerogels. The first step, at low temperatures from 30 to 300 $^{\circ}\text{C}$, the second stage at middle temperatures between 300 and 500 $^{\circ}\text{C}$, and the final step from 500 to 850 $^{\circ}\text{C}$. Peaks detected at low temperatures are assigned to the evaporation of residual, small molecules, such as water, ethanol, unreacted silanols, or molecules from scissions of the unstable head-to-head linkages [18–21]. The second stage is originated from the degradation of organic chains of siloxanes, therefore xerogels with more proportion of organic compound (GPTMS), TG12, has higher intensity on the first derivate peak and the maximum of these peaks is displaced to lower

temperaturas (Table 3). The final degradation percentage (Ta 850 °C) is higher with the increase of organic proportion in the xerogel formulation (Table 3) due to the increase of organic changes, which are susceptible of been degraded between the studied temperature ranges. The inorganic structure of the three syntheses was characterized by ²⁹Si-NMR in solid state. Two kinds of signals can be identified, T_n and Q_m, where n and m gives the number of Si-O-Si bridging oxygen bonds for a central Si atom. The subscript n takes values from 0 to 3 for GPTMS while m has values from 0 to 4 for the inorganic compound TEOS [22]. The T_n signals, derived from GPTMS, appear in the rango -40 to -80 ppm and the signals Q_n from TEOS appear between -80 and -120 ppm. These chemical shifts correlate with the ones reported in the literature [22,23]. The absence of T₀ and Q₀ signals in the three xerogels corresponds to the non-condensable molecules of GPTMS and TEOS [21], which ensures a high cross-linkage of the sol-gel network. The good cross-linkage achieved in the three networks is confirmed with the identification of signals T₃ and Q₄. The relative proportions of T and Q peaks of the xerogels are listed in Table 4. The calculus of the relative proportions revealed that the local bonding environment of the silicon atoms are influenced by the starting amount of precursors [22]. The intensity of the peaks (Fig. 5), which are proportional to the abundance of T_n and Q_m species, reveal, as expected, that when adding more GPTMS than TEOS (TG12) the T_n signals contributed more to the averaging cross-linkage. However, when the quantity of the precursors GPTMS and TEOS was equal (TG11) the condensation from GPTMS was higher than TEOS [22]. It seems that GPTMS favors the condensation degree in silica network mainly due to its cross-linking capacity through the epoxy group [23,24].

Characterization of the coating

Fig. 6 shows the micrographs of the surface (A–C) and a cross-section (D–F) of each coating. At first glance, it can be observed that the three syntheses completely cover the surface of the carbon Steel substrate. There are remarkable differences between the surface of each coating (Fig. 6(A–C)), TG12 presents a uniform surface without cracks, while coatings TG11 and TG21 present considerable cracks. Equal or higher proportions of the inorganic silane, TEOS, created tensions on the surface that ended up in the formation of cracks. The transversal section of the different specimens showed that coatings had a homogenous and constant thickness with values that ranged between 47 to 93 μm (Table 5). Accordingly to what was observed with the Surface inspection, TG11 and TG21 exhibit also cracks from the surface of the coating to the metal. Coating TG12 is the solely coating free of cracks and defects that can ensure a good protection of the metallic substrate [25]. The water contact angle of the modified surfaces was also studied and values are shown in Table 5. The uncoated metallic substrate was studied and taken as reference. The application of the sol-gel coatings to the substrate modified the nature of the surface from hydrophobic to hydrophilic surfaces. Coatings TG11 and TG21 had similar contact angle values, however, the coating with more GPTMS, TG12, presents an increase on the water contact angle value due to the presence of more organic precursor. The hydrophilicity of the sol-gel coatings is influenced by two main factors; the chemical composition and the microstructure of the solid face [26]. The adsorptions of polar molecules like water on the surface of coatings are promoted by the presence of Si-OH groups in the xerogel structure. The presence of more Si-R groups instead of Si-OH groups, inhibits the adsorption of water increasing the hydrophobicity of coatings, as it happens in coating TG12 due to its higher cross-linkage and low presence of Si-OH groups on its surface [27,28].

Evaluation of the corrosion resistance of coatings

Potentiodynamic polarization and electrochemical impedance spectroscopy (EIS) techniques were employed to evaluate the electrochemical profile of samples TG11, TG12, TG21 and the substrate without coating. The results of the potentiodynamic study are shown in Fig. 7. Corrosion current density (*i*_{corr}), corrosion potential (*E*_{corr}) and polarization resistance were

evaluated by analysing the anodic and cathodic curves using ANOVA analysis software and the values are presented in Table 6. The values of E_{corr} significantly shifted to more noble potentials when compared with the uncoated substrate. The coating TG12 presented the most positive corrosion potential meaning the application of TG12 on the steel acted as the best protective layer. The corrosion current density, i_{corr} , is directly related with the corrosion rate. The coatings also reduced the corrosion rate of the uncoated metal at different rates: the coating TG12 showed the lowest corrosion rate followed by coating TG21 and TG11.

Polarization resistances for coating TG12 is one order of magnitude compare to TG11 and TG21, revealing a higher efficiency for corrosion protection for the coating with higher ratio of organic silane compound. The percentage of inhibition of coatings to electrochemical corrosion, PI, was calculated using the Eq. (1) proposed by Yuet et al. [29,30].

Where i_{corr} and i_{corr}^0 are the corrosion current densities in the presence of the coating and the bare metal, respectively. Table 6 shows the results of the PI of the three samples. Despite the presence of cracks

$$PI(\%) = 100 \times \left(1 - \frac{i_{corr}}{i_{corr}^0}\right)$$

on coatings TG11 and TG21, they considerably inhibited the electrochemical corrosion, being the coating TG21 thicker than coating TG11 the one providing better inhibition. The presence of cracks and defects on the coatings TG21 and TG11 provide a path for diffusion of corrosive species such as water, oxygen and chloride ions to the coating/metal interface [31] while the crack-free coating TG12 present the highest inhibitor percentage [32]. The corrosion resistance of the coatings was also evaluated with EIS. Fig. 8 displays EIS data by Nyquist (complex vs real impedance) and Bode (impedance modulus and phase angle vs frequency) plots of the samples of the silane coatings prepared and the bare metal after 24, 48 and 72 h exposed to an aqueous solution containing 10mM of NaCl. Tests were recorded at their corresponding open circuit potential (OCP) after 24 h immersed in the testing solution. Before and after each impedance test, the OCP was recorded and differences between the starting and the final OCP remained smaller than 50 mV in all cases. Despite the diagrams presented in Fig. 8 shows a significant difference between the coated and uncoated panels, one equivalent circuit (EC) was used to fit all the samples (Fig. 9). The circuit elements of the four samples are given in Table 7. The chi-square (χ^2) values for the simulations were of the order 10⁻³ and confirm the validity of the fitting. The uncoated steel sample shows two constant times in parallel. The equivalent circuit consists on the resistance of the electrolyte, R_s , representing the resistance between the working and the reference electrode; in series the first constant time at high frequencies is represented by a constant phase element (CPE_f) and its resistance (R_f), which is associated to the interface electrolyte/metal; and the second constant time at low frequencies is represented by CPE_o and its resistance (R_o), which indicates the presence of oxide due to the corrosion process. The electrochemical feature of the coatings had the same features showing two constant times. At high frequencies the first constant time is attributed to the barrier properties of the coating and the second one to the corrosion process that occurs in the interface electrolyte/metal once the electrolyte achieve the metallic surface due to the presence of pores or the degradation of the coating [33,16]. EIS data were analyzed using the equivalent circuit given in Fig. 9 where R_s represents the electrolyte resistance CPE_f the constant phase element related with the film capacitance, R_f , the film resistance, CPE_o the constant phase element related with the interface electrolyte/metal and its resistance R_o . First, Bode diagram allows confirming that all the coatings acted as a protective layer of the carbon steel substrate because its resistance was considerably improved. Coating TG21 only enhance the resistance of the carbon steel one order of magnitude whereas, coating TG12 increased almost 3 orders of magnitude the resistance of the bare metal. The resistance of the coating, R_f , has an extremely low value (Table 7) for coatings TG11 and TG21 systems comparing to TG12 after 24, 48 and 72 h of immersion. The low R_f values of coatings TG11 and TG21 are due to the presence of cracks where the electrolyte can achieve the metallic surface. The presence of cracks was previously corroborated with SEM characterization [33].

In addition, the averaging impedance of the coating TG12 is one and two orders of magnitude higher than the registered in coatings TG11 and TG21, respectively. Despite presenting the highest resistance among the studied specimens, coating TG12 considerably decreased its barrier properties within time as it was evidenced by the decrease of the amplitude arc (Nyquist diagram, Fig. 8(E)) and the impedance modulus (Bode diagram, Fig. 8(F)). Even though TG12 reduced its barrier properties with time, the obtained impedance was always the other coatings.

The uncoated steel system present low corrosion resistance highlighted by the low polarisation resistance (R_f) which is about $500 \Omega\text{cm}^2$. The polarization resistance of the three coatings is higher than the one of the uncoated steel, this can be evidenced in the increase on the amplitude in Nyquist diagram and in the increase on the impedance value in Bode diagram. This indicates that the uncoated steel experiences a quick corrosion process, which is effectively retarded when sol-gel coatings are applied on its surface.

Conclusions

Three sol-gel coatings were applied on carbon steel substrates by varying the molar ratio of the precursors GPTMS and TEOS. This study concludes that hydrolysis and condensation reactions are not dependent on the molar ratio, since signals on FTIR reveal the absorption bands related to these reactions and the evolution of the viscosity is similar through time. The thermogravimetric study revealed that the presence of the organosilane did not alter the formation of siloxane bonds since the mass loss of each xerogel correlates with the organic content. However, the presence of more organosilane (GPTMS) influenced the chemical entourage of the Si atoms by assisting the creation of siloxane bonds through the opening of the epoxy group. Additionally, the presence of more GPTMS generated a surface with higher water contact angles. The SEM superficial inspection reveals a growth of cracks on a nonhomogeneous surface with the decrease of the organosilane GPTMS. On the contrary, coating TG12 has no defects on its surface due to the flexibility offered by the organic compound that reduces superficial tensions on the curing process. This coating also presents higher water contact angle in order to repel water contact, and intermediate thickness. The barrier features of the coatings were studied by means of potentiodynamic polarization and EIS. The electrochemical study confirmed that coating TG12, which had the most suitable surface characteristics, is the most protective coating for carbon steel substrates. Cracks and defects on the surface of TG11 and TG21 might allow penetration of electrolyte achieving metal surface where corrosion process might start; this is evidence on the lower values of the resistance of charge transfer (R_o) compared to TG12. Higher proportion of organic precursor, improves barrier properties for corrosion protection. The author(s) declared no potential conflicts of interest with respect to the research, authorship, and/or publication of this article.

Acknowledgements

The authors acknowledge the financial support from the Regional Government of Madrid through the program MULTIMAT-CHALLENGE (S2013/MIT-2862). The authors acknowledge the financial support from the European Union and Government of Spain through the program RETOS COLABORACION. RECORD (RTC-2015-3513-S)

References

- [1] M. Hernandez-Escolano, X. Ramis, A. Jimenez-Morales, M. Juan-Diaz, J. Suay, Study of the thermal degradation of bioactive sol-gel coatings for the optimization of its curing process, *J. Therm. Anal. Calorim.* 107 (2) (2012) 499–508.
- [2] G.W. Walter, A critical review of the protection of metals by paints, *Corros. Sci.* 26 (1) (1986) 27–38 Jan..
- [3] A.A. El Hadad, D. Carbonell, V. Barranco, A. Jimenez-Morales, B. Casal, J.C. Galvan, Preparation of sol-gel hybrid materials from γ -methacryloxypropyltrimethoxysilane and tetramethyl orthosilicate: study of the hydrolysis and condensation reactions, *Colloid Polym. Sci.* 289 (17–18) (2011) 1875–1883.
- [4] T. Lutzler, T.V.J. Charpentierb, R. Barkera, S. Soltanahmadia, W. Taleba, C. Wanga, A. Alejo-Rodriguezc, E. Perrec, H. Schneiderc, A. Nevillea, Evaluation and characterization of anti-corrosion properties of sol-gel coating in CO₂ environments, *Mater. Chem. Phys.* 216 (2018) 272–277 Sep.

- [5] M. Bahrami, G.H. Borhani, S.R. Bakhshi, A. Ghasemi, Preparation and evaluation of corrosion behavior of GPTMS–TEOS hybrid coatings containing Zr and Ce on aluminum alloy 6061-T6, *J. Solgel Sci. Technol.* 76 (3) (2015) 552–561 Dec.
- [6] S. Yaacoub, S. Calas, J. Jabbour, R. Tauk, D. Zaouk, A. Khoury, P. Etienne, Study of the mechanical properties of two organic-inorganic hybrid systems: GPTMS/coloidal silica and GPTMS/TEOS, *J. Non. Solids* 358 (22) (2012) 3036–3041.
- [7] E. Alibakhshi, M. Akbarian, M. Ramezanzadeh, B. Ramezanzadeh, M. Mahdavian, Evaluation of the corrosion protection performance of mild steel coated with hybrid sol-gel silane coating in 3.5 wt.% NaCl solution, *Prog. Org. Coatings* 123 (2018) 190–200 Oct..
- [8] A.-P. Romano, M. Fedel, F. Deflorian, M.-G. Olivier, Silane sol-gel film as pretreatment for improvement of barrier properties and filiform corrosion resistance of 6016 aluminium alloy covered by cathodic coating, *Prog. Org. Coatings* 72 (4) (2011) 695–702 Dec..
- [9] M. Taheri, R. Naderi, M. Saremi, M. Mahdavian, Development of an ecofriendly silane sol-gel coating with zinc acetylacetonate corrosion inhibitor for active protection of mild steel in sodium chloride solution, *J. Solgel Sci. Technol.* 81 (1) (2017) 154–166 Jan..
- [10] D. Wang, G.P. Bierwagen, Sol-gel coatings on metals for corrosion protection, *Prog. Org. Coatings* 64 (4) (2009) 327–338 Mar..
- [11] R.B. Vignesh, J. Balaji, M.G. Sethuraman, Surface modification, characterization and corrosion protection of 1,3-diphenylthiourea doped sol-gel coating on aluminium, *Prog. Org. Coatings* 111 (May) (2017) 112–123.
- [12] E.K. Kim, J. Won, J. young Do, S.D. Kim, Y.S. Kang, Effects of silica nanoparticle and GPTMS addition on TEOS-based stone consolidants, *J. Cult. Herit.* 10 (2) (2009) 214–221.
- [13] K.H. Wu, C.M. Chao, T.F. Yeh, T.C. Chang, Thermal stability and corrosion resistance of polysiloxane coatings on 2024-T3 and 6061-T6 aluminum alloy, *Surf. Coatings Technol.* 201 (12) (2007) 5782–5788.
- [14] P.H. Suegama, I.V. Aoki, Electrochemical behavior of carbon steel pre-treated with an organo functional bis-silane filled with copper phthalocyanine, *J. Braz. Chem. Soc.* 19 (4) (2008) 744–754.
- [15] L.M. Rueda, C. Nieves, C.A. Hernandez Barrios, A.E. Coy, F. Viejo, Design of TEOSGPTMS sol-gel coatings on rare-earth magnesium alloys employed in the manufacture of orthopaedic implants, *J. Phys. Conf. Ser.* 687 (2016) 012013.
- [16] F. Romero-Gavilan, S. Barros-Silva, J. Garcia-Canadas, B. Palla, R. Izquierdo, M. Gurruchaga, I. Gonib, J. Suay, Control of the degradation of silica sol-gel hybrid coatings for metal implants prepared by the triple combination of alkoxysilanes, *J. Non. Solids* 453 (2016) 66–73.
- [17] C. Agustin-Saenz, J.A. Sanchez-Garcia, M. Machado, M. Brizuela, O. Zubillaga, A. Tercjak, Broadband antireflective coating stack based on mesoporous silica by acid-catalyzed sol-gel method for concentrated photovoltaic application, *Sol. Energy Mater. Sol. Cells* 186 (2018) 154–164 Nov.
- [18] H. Li, S. Liu, J. Zhao, D. Li, Y. Yuan, Thermal degradation behaviors of polydimethylsiloxane-graft-poly(methyl methacrylate), *Thermochim. Acta* 573 (2013) 32–38.
- [19] G. Camino, S.M. Lomakin, M. Lagueard, Thermal polydimethylsiloxane degradation. Part 2. The degradation mechanisms, *Polymer (Guildf)* 43 (7) (2002) 2011–2015.
- [20] M. Criado, I. Sobrados, J. Sanz, Polymerization of hybrid organic-inorganic materials from several silicon compounds followed by TGA/DTA, FTIR and NMR techniques, *Prog. Org. Coatings* 77 (4) (2014) 880–891.
- [21] A. Alcantara-Garcia, A. Garcia-Casas, A. Jimenez-Morales, Electrochemical study of the synergic effect of phosphorus and cerium additions on a sol-gel coating for Titanium manufactured by powder metallurgy, *Prog. Org. Coatings* (2018) Feb.
- [22] Ruben F.A.O. Torrico, Samarah V. Harb, Addressa Trentin, Mayara C. Uvida, Sandra H. Pulcinelli, Celso V. Santilli, Peter Hammer, Structure and properties of epoxysiloxane- silica nanocomposite coatings for corrosion protection, *J. Colloid Interface Sci.* 513 (2018) 617–628 Mar.
- [23] D.R. Vollet, L.A. Barreiro, C.E.T. Paccola, C.M. Awano, F.S. de Vicente, M. Yoshida, D.A. Donatti, A kinetic modeling for the ultrasound-assisted and oxalic acid-catalyzed hydrolysis of 3-glycidoxypropyltrimethoxysilane, *J. Solgel Sci. Technol.* 80 (3) (2016) 873–880 Dec.
- [24] M.A. Robertson, R.A. Rudkin, D. Parsonage, A. Atkinson, Mechanical and thermal properties of organic/inorganic hybrid coatings, *J. Solgel Sci. Technol.* 26 (1/3) (2003) 291–295.
- [25] P.A. Sorensen, S. Kiil, K. Dam-Johansen, C.E. Weinell, Anticorrosive coatings: a review, *J. Coatings Technol. Res.* 6 (2) (2009) 135–176 Jun.
- [26] A. Venkateswara Rao, G.M. Pajonk, Effect of methyltrimethoxysilane as a co-precursor on the optical properties of silica aerogels, *J. Non. Solids* 285 (1–3) (2001) 202–209.
- [27] S.S. Latthe, H. Hirashima, A.V. Rao, TEOS based water repellent silica films obtained by a co-precursor sol-gel method, *Smart Mater. Struct.* 18 (9) (2009) 095017 Sep..
- [28] P.B. Wagh, S.V. Ingale, S.C. Gupta, Comparison of hydrophobicity studies of silica aerogels using contact angle measurements with water drop method and adsorbed water content measurements made by Karl Fischer's titration method, *J. Solgel Sci. Technol.* 55 (1) (2010) 73–78 Jul..
- [29] Y.J. Yu, J.G. Kim, S.H. Cho, J.H. Boo, Plasma-Polymerized Toluene Films for Corrosion Inhibition in Microelectronic Devices, (2003).

- [30] G. Ramirez, S.E. Rodil, H. Arzate, S. Muhl, J.J. Olaya, Niobium based coatings for dental implants, *Appl. Surf. Sci.* 257 (7) (2011) 2555–2559 Jan..
- [31] R. Suleiman, M. Khaled, H. Wang, T.J. Smith, J. Gittens, R. Akid, B. Mohamad El Ali, A. Khalil, Comparison of selected inhibitor doped sol-gel coating systems for protection of mild steel, *Corros. Eng. Sci. Technol.* 49 (3) (2014) 189–196.
- [32] A. Duran, Y. Castro, M. Aparicio, a. Conde, J.J. de Damborenea, Protection and surface modification of metals with sol-gel coatings, *Int. Mater. Rev.* 52 (3) (2007) 175–192.
- [33] K. Joncoux-Chabrol, J.P. Bonino, M. Gressier, M.J. Menu, N. Pebere, Improvement of barrier properties of a hybrid sol-gel coating by incorporation of synthetic talclike phyllosilicates for corrosion protection of a carbon steel, *Surf. Coatings Technol.* 206 (11–12) (2012) 2884–2891.

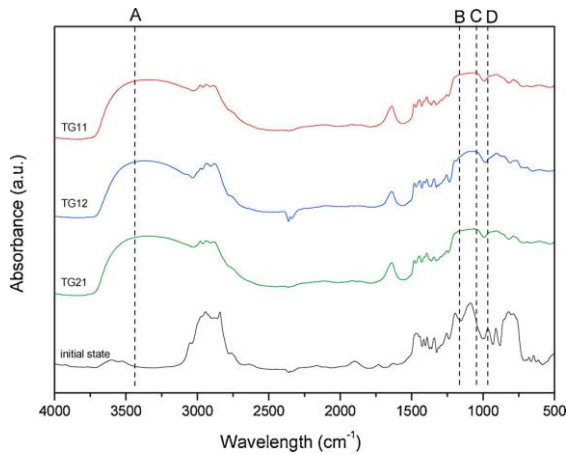


Fig. 2. FTIR spectra of synthesis TG11 before water addition; and syntheses TG11, TG12 and TG21 at 24 h of synthesis

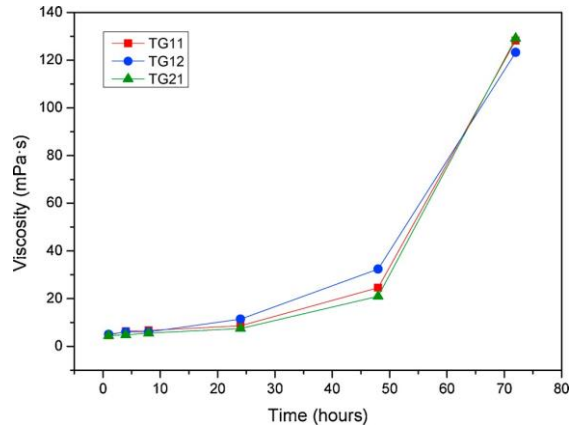


Fig. 3. Evolution of the viscosity with time (1, 4, 8, 24, 48 and 72 h) for synthesis TG11, TG12 and TG21.

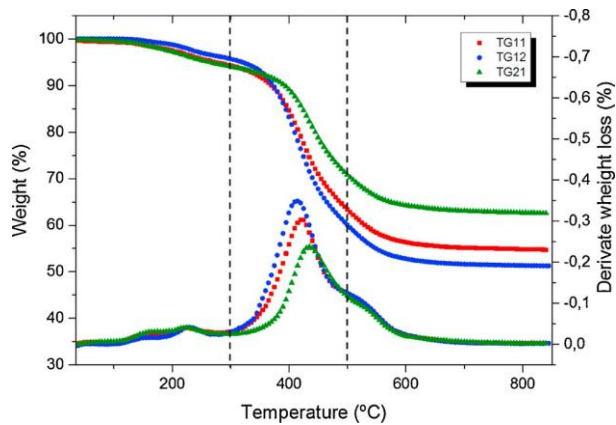


Fig. 4. Thermogravimetric analyses and their first derivate for xerogels TG11, TG12 and TG21.

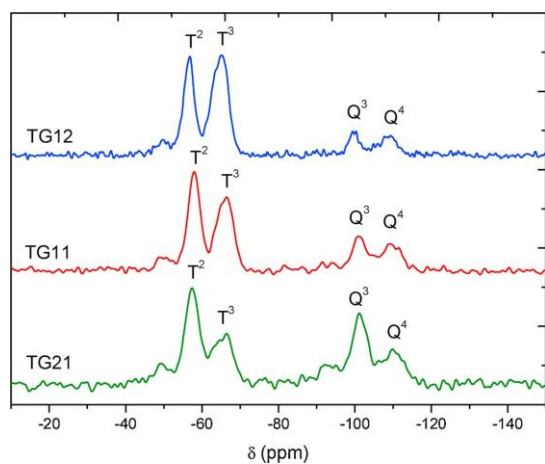


Fig. 5. Solid state ^{29}Si -NMR spectra of xerogels from synthesis TG11; TG12; TG21

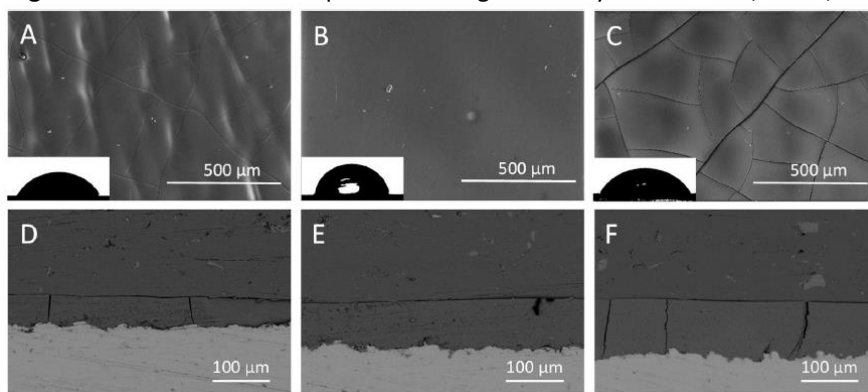


Fig. 6. SEM micrographs of the surface of coatings and contact angle (A-C) and transversal section (D-F) prepared with synthesis TG11 (A and D); TG12 (B and E); TG21 (C and F).

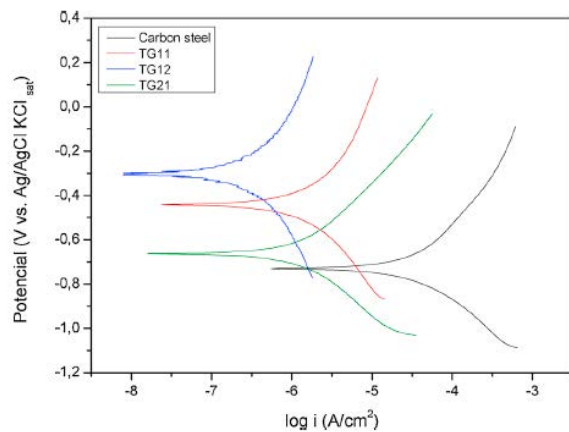


Fig. 7. Line polarization of the uncoated substrate and coatings TG11, TG12, TG21.

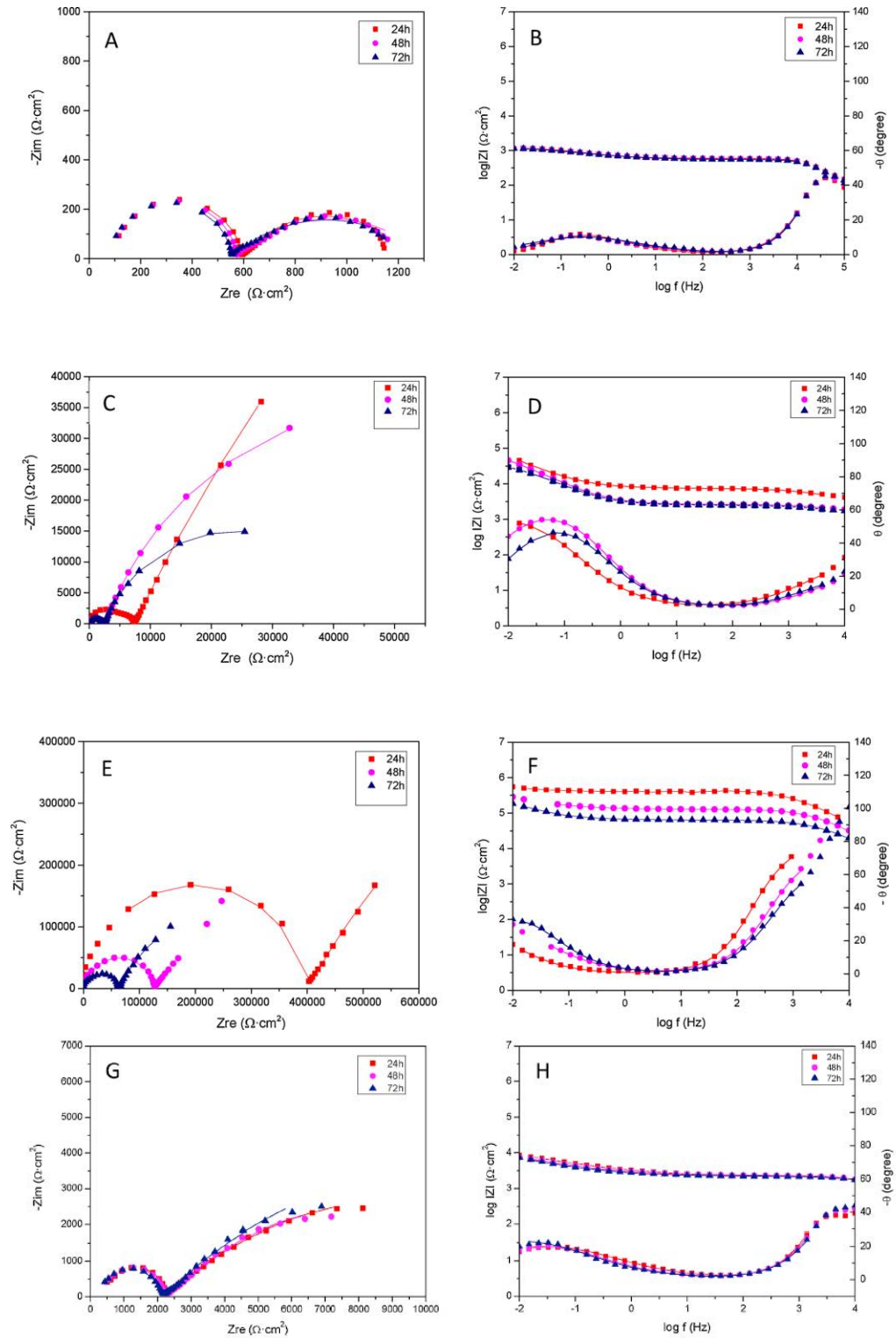


Fig. 8. Measured (discrete points) and fitted (solid lines) impedance spectrum of coatings: A–B) uncoated steel C–D) coating TG11; E–F) coating TG12; G–H) coating TG21 after 24, 48 and 72 h of exposure to 10mM NaCl solution. Frequency range applied: 104 Hz to 10⁻² Hz.

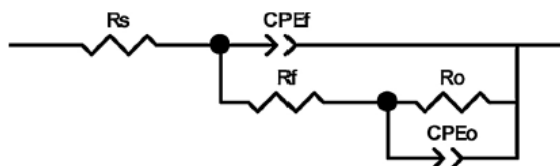


Fig. 9. Equivalent circuit used to fit the impedance data of the uncoated steel, and coatings TG11, TG12, TG21.

Table 2
Assignment of FTIR peaks of Fig. 2.

Signal	Wavelength (cm ⁻¹)	Hydrolysis	Condensation
A	3300-3500	v _{OH} (Si-OH/H ₂ O)	
B	1163		v _s (Si-O-Si)
C	1054		Si-O-Si
D	950	Si-OH	

Table 3
Thermogravimetric data from TGA curves for xerogels TG11, TG12, and TG21.

Xerogel	T ₂ ^b / °C	Organic %
TG11	419.9	41.8
TG12	414.7	46.9
TG21	434.7	34.4

T₂^b: Temperature of the second degrading step.

Table 4
Relative proportions and ratio of Tⁿ and Q^m signals calculated for each xerogel form ²⁹Si-NMR spectra of Fig. 5.

Xerogel	Relative proportion ^a %				Ratio ^b %	
	T ²	T ³	Q ³	Q ⁴	T ⁿ	Q ^m
TG11	43	32	14	11	75	25
TG12	41	41	10	9	82	19
TG21	39	20	28	13	59	41

^arelative proportion (%): $T^i = (T^i / (\sum_{i=2}^3 T + \sum_{j=3}^4 Q)) \cdot 100$.

$Q^j = (Q^j / (\sum_{j=3}^4 Q + \sum_{i=2}^3 T)) \cdot 100$.

^bratio (%): $T^n = (\sum_{i=1}^3 T / (\sum_{i=1}^3 T + \sum_{j=2}^4 Q)) \cdot 100$.

$Q^m = (\sum_{j=2}^4 Q / (\sum_{i=1}^3 T + \sum_{j=2}^4 Q)) \cdot 100$.

Table 5
Values of the thickness of the coatings and contact angle degrees.

Coating	Thickness (µm)	Water contact angle (degrees)
Uncoated steel	-	107.2 ± 4.4
TG11	47.6 ± 3.3	61.1 ± 2.7
TG12	77.8 ± 7.2	77.4 ± 6.4
TG21	92.8 ± 4.4	61.9 ± 3.7

Table 6
Values of the Tafel analysis.

Sample	I corr (A)	i corr (A/cm ²)	E corr (V)	Polarization resistance (kΩcm ²)	PI (%)
Uncoated Steel	2.5E-1	6.7E-1	-0.75	0.8	-
TG11	6.2E-3	1.6E-2	-0.44	51.7	97.6
TG12	2.3E-4	6.0E-4	-0.30	298.8	99.9
TG21	1.3E-3	3.4E-3	-0.66	47.4	99.5

Table 7
Circuit elements of the silane coated steel immersed in 10 mM NaCl until 72 h.

	Time (h)	Log Z _{Lf}	R _f (Ωcm ²)	CPE _{r-T1} (Fcm ⁻²)	CPE _{r-P1}	R _o (Ωcm ²)	CPE _{o-T2} (Fcm ⁻²)	CPE _{o-P2}	Chi-Sqr x 10 ⁻³
Steel	24	3.1	506	3,30E-08	0.95	625	1,40E-03	0.63	1.6
	48	3.1	456	4,40E-08	0.98	739	1,50E-03	0.52	0.9
	72	3.1	419	2,00E-08	1.01	754	1,46E-03	0.5	0.6
TG12	24	5.7	415000	1,33E-09	0.86	684000	3,39E-05	0.75	4.2
	48	5.5	130000	2,89E-09	0.83	1290000	2,57E-05	0.6	0.9
	72	5.3	63100	6,21E-09	0.81	412000	4,11E-05	0.7	1.1
TG11	24	4.7	9000	2,04E-07	0.56	424000	1,24E-04	0.72	0.8
	48	4.7	3190	2,13E-07	0.59	98700	1,53E-04	0.78	0.2
	72	4.5	2990	3,78E-07	0.56	43200	1,78E-04	0.77	0.4
TG21	24	3.9	1820	1,25E-08	0.94	14300	3,43E-04	0.46	0.1
	48	3.9	2490	3,14E-08	0.79	12300	4,72E-04	0.49	0.4
	72	3.9	2750	3,47E-08	0.75	17400	5,65E-04	0.49	0.8